

The Urban Heat Island Under Climate Change: Analysis of Representative Urban Blocks in Northwestern Italy

Original

The Urban Heat Island Under Climate Change: Analysis of Representative Urban Blocks in Northwestern Italy / Piro, Matteo; Ballarini, Ilaria; Pourabdollahtookaboni, Mamak; Corrado, Vincenzo; Pernigotto, Giovanni; Borelli, Gregorio; Gasparella, Andrea. - In: ENERGIES. - ISSN 1996-1073. - ELETTRONICO. - 19:3(2026), pp. 1-25.
[10.3390/en19030660]

Availability:

This version is available at: 11583/3007154 since: 2026-02-24T13:17:57Z

Publisher:

MDPI

Published

DOI:10.3390/en19030660

Terms of use:








This article is made available under terms and conditions as specified in the corresponding bibliographic description in the repository

Publisher copyright

(Article begins on next page)

Article

The Urban Heat Island Under Climate Change: Analysis of Representative Urban Blocks in Northwestern Italy

Matteo Piro ¹, Iliaria Ballarini ^{1,*}, Mamak P. Tootkaboni ¹, Vincenzo Corrado ¹, Giovanni Pernigotto ²,
Gregorio Borelli ² and Andrea Gasparella ²

¹ TEBE Research Group, Department of Energy “Galileo Ferraris”, Politecnico di Torino, Corso Duca degli Abruzzi 24, 10129 Turin, Italy; matteo.piro@polito.it (M.P.); mamak.ptootkaboni@polito.it (M.P.T.); vincenzo.corrado@polito.it (V.C.)

² Faculty of Engineering, Free University of Bozen-Bolzano, via Bruno Buozzi 1, 39100 Bolzano, Italy; giovanni.pernigotto@unibz.it (G.P.); gregorio.borelli@student.unibz.it (G.B.); andrea.gasparella@unibz.it (A.G.)

* Correspondence: ilaria.ballarini@polito.it; Tel.: +39-011-090-4549

Abstract

Urban populations are exposed to elevated local temperatures compared to surrounding rural areas due to the urban heat island (UHI) effect, which increases health risks and energy demand. The literature highlights that accurately quantifying UHIs at broader territorial scales remains challenging because of limited microscale climate data availability and, at the same time, the difficulty of increasing the spatial coverage of the outcomes. Within the PRIN2022-PNRR CRiStAll (Climate Resilient Strategies by Archetype-based Urban Energy Modeling) project, this work addresses these limitations by coupling Urban Building Energy Modeling with archetype-based representation of urban form and high-resolution climatic data. Urban archetypes are defined as representative microscale configurations derived from combinations of urban canyon geometries and building typologies, accounting for different climatic zones, use categories, and construction periods. The proposed methodology was applied to the city of Turin (Italy), where representative urban blocks were identified and modeled to evaluate key urban context metrics under short-, medium-, and long-term climate scenarios. The UHI effect was assessed using Urban Weather Generator, while energy simulations were performed with CitySim. The urban archetype approach enables both fine spatial resolution and extensive spatial coverage, supporting urban-scale mapping.

Keywords: urban heat island; climate change; urban building energy modeling; archetype-based approach; urban archetype; future weather files



Academic Editor: Paulo Santos

Received: 22 December 2025

Revised: 16 January 2026

Accepted: 25 January 2026

Published: 27 January 2026

Copyright: © 2026 by the authors.

Licensee MDPI, Basel, Switzerland.

This article is an open access article

distributed under the terms and

conditions of the [Creative Commons](https://creativecommons.org/licenses/by/4.0/)

[Attribution \(CC BY\)](https://creativecommons.org/licenses/by/4.0/) license.

1. Introduction

1.1. Background Analysis and Literature Review

Today, more than half of the world’s population resides in cities, with urbanization continuing to grow at an unprecedented pace. Predictions indicate that 68% of the world’s population will live in cities by 2050 [1]. With cities consuming more than 60% of the world’s resources and contributing around 70% of global carbon emissions, this rapid urbanization raises concerns for sustainable planning and management [2]. Rapid urbanization is also associated with several other challenges. Particularly, continued urban expansion appears to intensify the urban heat island (UHI) effect through interactions with

mesoscale atmospheric forces and its influence on broader urban metabolic processes. Recent investigations emphasize that the acceleration of urban growth has amplified thermal stress in densely built areas, particularly in Mediterranean and mid-latitude contexts, where compact urban forms and limited vegetation reinforce local warming [3]. Studies have also highlighted that rapid land-use transitions tend to modify surface energy budgets, increasing sensible heat fluxes and reducing urban cooling capacity [4].

The World Meteorological Organization (WMO) [5] defines a UHI as the “*observed difference in temperature between an urban area and its surrounding non-urban areas under comparable synoptic conditions*”. The UHI is caused by an energy imbalance linked to surfaces with heat-absorbing materials, reduced evapotranspiration, and anthropogenic heat release, all contributing to elevated temperatures [6]. This impact can vary based on different factors and geographical context. For example, empirical research in Rome has shown that UHI intensities can surpass 4 °C and lead to an increase in cooling energy demand by up to 81% and decrease heating demand by 33% [7,8]. In another study, microclimate simulations of several European neighborhoods suggest that excluding UHI leads to an underestimation of cooling loads by around 10% [9]. Recent studies also point to the likelihood that the combined effects of urbanization and climate change will intensify extreme heat events [10]. These findings suggest that incorporating UHI dynamics into assessments of building energy performance is essential under both current climate conditions and in future scenarios.

Evaluating urban microclimate characteristics and analyzing the energy behavior of building stocks are crucial in investigating UHI. Accordingly, it is useful to make a distinction between the urban canopy layer (UCL) and the urban boundary layer (UBL), which corresponds to the separation between micro- and meso-scale atmospheric processes [11]. The microscale and site-specific factors that control airflow and energy exchange influence the UCL, which extends from the ground to the roof level. On the other hand, the UBL, located above building height, belongs to the planetary boundary layer and is influenced by the urban surface or land-use zones below it. Analyses of urban microclimates also need to account for anthropogenic heat emissions, including those from traffic and building systems, which can substantially modify thermal conditions within urban canyons [12].

Moreover, morphological parameters such as street width, building height, surface coverage, and vegetation strongly influence the UCL. For instance, increases in canyon aspect ratio or surface coverage can increase cooling loads, likely due to reduced within-canyon ventilation [13]. Similarly, denser urban fabrics can limit natural ventilation potential, although the magnitude of this effect varies based on the local climate and prevailing wind regimes [3]. In this context, a representative-block approach, which groups urban configurations by key metrics, helps capture this heterogeneity and facilitates microscale climate modeling [9]. In the same vein, how building stocks are represented in urban-scale energy analyses becomes another important consideration.

Urban building energy modeling (UBEM) [14] is commonly used to evaluate urban energy performance and analyze the energy interaction between buildings and their surroundings. UBEM uses a bottom-up methodology that is usually classified into statistical, hybrid, and engineering (i.e., physical-based methods). Building archetypes are especially prevalent among physical-based methods that enable us to show how a place adopts sustainable and energy-efficient policies and how it responds to climate change. This is conducted by combining both technological innovations and the cultural identity of that context. In this approach, building stocks are divided into comparable groups in modeling according to factors like building categories, construction periods, climatic zones, or other relevant criteria. Archetype schemes are then used to characterize these groups by their energy performance features [15].

Many studies on the evolution of building archetypes can be found in the literature. For instance, the Italian research project PRIN2020 URBEM (Urban Reference Buildings for Energy Modeling) aims to develop a national database of archetype buildings [16]. Another study, conducted by Sousa Monteiro et al. [17], investigated the Portuguese residential building stock in Lisbon, where the authors combined census, GIS, and municipal datasets to improve the representativeness of archetype groups. Johari et al. [18] used Swedish representative buildings generated from energy performance certificates to validate and calibrate the UBEM. Furthermore, for residential homes in Kuwait City, Cerezo et al. [19] investigated probabilistic and deterministic building archetypes.

Although it is commonly known that the UHI effect significantly affects building energy performance, only a small number of studies have been successful in precisely quantifying this variation due to the challenges in both gathering microscale climatic data (UCL analysis) and modeling the drivers of UHI while accounting for interactions between buildings and their surroundings (UBEM). The energy balance at the UCL [6,20] and the dynamical numerical techniques (computational fluid dynamics) [21,22] yielded the most reliable results among these models. However, using microscale models for a district or a whole city with all its characteristics and geometries is often not feasible due to the huge computing cost. At the same time, due to the lack of climate data with both broader spatial coverage (i.e., detailed mapping of urban areas) and finer spatial resolution (i.e., microscale measurements), UBEM typically fails to effectively address the UHI. To better explore the UHI impacts, researchers often use archetypes. This approach involves defining typical urban configurations by incorporating local microclimatic conditions into representative urban forms. These efforts enhance the robustness of archetype-based modeling and better support the development of UHI-sensitive mitigation and adaptation strategies [23].

In this context, recent research has shown that representative urban forms can be obtained by morphological indicators such as plan area density, site-coverage ratio, aspect ratio, and average building height, which strongly influence local UHI intensity and ventilation potential [13,24]. Moreover, studies comparing compact, mid-rise, and open-low-rise configurations demonstrate that district geometry directly shapes the microclimatic conditions [9]. Therefore, incorporating such morphology-dependent microclimate modifications into archetypal blocks enables UBEM workflows to more accurately represent the spatial variability of UHI impacts and identify which urban textures exacerbate or mitigate overheating risks. Integrating urban morphology into archetype-based models helps identify adaptation methods like increasing vegetation, improving surface reflectivity, or adjusting density based on local climatic conditions.

Finally, the importance of examining how UHI interacts with ongoing climate change and urbanization is increasingly recognized, as their combined effects play a major role in shaping building energy performance [25]. Recent works have started to address this combined effect. Shen et al. [26] developed a method to project hourly urban air temperatures by coupling global climate models with local UHI conditions and observed that climate change amplified UHI intensity and reduced heating degree days. Another study in three Chinese megacities showed that the combined effect of UHI and climate change could increase annual cooling demand by up to 100% [27]. In the Midwestern U.S., Hashemi et al. [28] reported that including UHI and future climate scenarios will increase cooling energy use by 91% by 2050 and 154% by 2080. In Auckland, Jalali et al. [29] found that UHI and climate change together raised the cooling demand by up to 23%. Keppas et al. [30] projected stronger nocturnal UHI under Mediterranean climate scenarios, with urban minimum temperatures exceeding rural values by about 1.5–3 °C during summer nights. Finally, Lu et al. [31] used climate projections from CMIP6, the latest phase of the Coupled Model Intercomparison Project [32], together with downscaling techniques, to assess future urban

thermal conditions and the role of land-use characteristics and nature-based solutions in shaping them. Their results emphasize that future climate assessments need to integrate both global climate forcing and locally specific urban processes. These studies reflect the importance of developing climate datasets that integrate climate change projections with neighborhood-scale urban characteristics, enabling more realistic evaluations of future building energy performance.

1.2. Aim of the Research

The literature background overview highlights that accurately quantifying UHIs at broader territorial scales remains challenging because of limited microscale climate data availability—either historical data or considering future projections—as well as the difficulty of increasing the spatial coverage of the outcomes due to heterogeneous urban forms. In addition, existing archetype-based UBEM studies often rely on predefined, idealized, or parametrically varied configurations (e.g., compact/open, high-/low-rise), which limits their ability to derive representative urban blocks directly from the entire urban building stock.

The research gaps have to be overcome by answering to the simultaneous needs of:

- Incorporating local microclimatic conditions (UHI) into urban forms;
- Integrating urban morphology into archetype-based models;
- Coupling climate change projections with urban forms in climate datasets.

The present work addresses these needs by coupling urban building energy modeling with a data-driven archetype-based representation of urban forms and high-resolution climatic data—including present and future projections. The research has been performed within the PRIN2022-PNRR CRiStAll (Climate Resilient Strategies by Archetype-based Urban Energy Modeling) project, founded by the European Union through the NextGenerationEU initiative within the PRIN 2022 PNRR program of the Italian Ministry of University and Research [33].

In CRiStAll, a methodology to create urban archetypes has been developed; the urban archetypes are defined as representative microscale configurations derived from combinations of urban canyon geometries and building typologies, accounting for different climatic zones, use categories, and construction periods. In this study, representative urban blocks were first identified through quantitative geometry-based metrics and statistical reduction techniques, and subsequently prioritized using ECOSTRESS-derived land surface temperature to identify those that were both geometrically representative and more vulnerable to UHI effects. The UHI effect is incorporated within the urban blocks using Urban Weather Generator (UWG) by adopting current, mid-, and long-term urban weather files. Finally, key performance indicators were assessed by means of a UBEM tool (CitySim).

The proposed methodology was applied to the city of Turin (Italy), where representative urban blocks were identified and modeled to evaluate key urban context metrics under short-, medium-, and long-term climate scenarios.

The article is organized as follows. In Section 2, the overall methodology developed in CRiStAll is presented, providing insight into the definition of the urban archetypes and the setting of key performance indicators assessed in the work. In Section 3, the application of the method to the city of Turin is provided, and the outcomes are presented and discussed in Section 4. Finally, the conclusions are drawn in Section 5.

2. Methodology

2.1. Overview of the CRiStAll Project

The CRiStAll research project [33] focuses on the following three research lines:

- Developing urban climate models that incorporate short-, medium-, and long-term climate change projections (future weather data) as well as micro-scale UHI effects (A);
- Implementing an archetype-based UBEM using representative urban context configurations (B);
- Evaluating the impact of climate-resilient and UHI-mitigating strategies in urban environments (C).

The relationships among these three research lines can be summarized as follows:

- (A–B) The micro-scale urban climate model is developed by considering the morphology, surface materials, and building geometries of the representative urban configurations;
- (B–C) The UBEM, built on building archetypes within these typical contexts, is enhanced by integrating climate-resilient and UHI mitigation strategies;
- (C–A) The effects of these strategies are considered in the urban climate model.

Despite these interrelationships, each research line can be developed separately from the others. To narrow the scope of analysis, in the present article, the CRiStAll methodology focused on research lines (A) and (B) to demonstrate how assessing micro-scale UHI under future climate conditions would benefit from the use of typical urban configurations in UBEM.

The consideration of climate resilient strategies (research line C) is not presented in the article because this will be developed in a subsequent phase of CRiStAll.

The implementation of the archetype-based UBEM using representative urban context configurations taking into account short-, medium-, and long-term climate change projections (future weather data), as well as micro-scale urban heat island effects, was carried out according to the following key activities:

- (1) Identification of representative urban archetypes using geometrical metrics;
- (2) Generation of current and future weather data incorporating UHI effects for each urban archetype;
- (3) Definition of key performance indicators (KPIs);
- (4) UBEM development and assessment of KPIs for each urban archetype and microclimate condition.

2.2. Geometrical Representativeness and Urban Archetypes

The first step was dedicated to the identification of districts with a geometry representative of the morphology of an urban settlement and, at the same time, meaningful for the study of the local UHI phenomena. The proposed methodology is a twofold procedure that ensures the integration of a detailed analysis of urban morphological characteristics with satellite-derived Land Surface Temperature (*LST*) data.

As far as the geometrical features are concerned, the workflow presented by Borelli et al. [34] was implemented. By aggregating a comprehensive dataset of the building cadastral parcels, usually consisting of all buildings in a city, urban blocks were derived. An initial data-cleaning activity was implemented to remove blocks (1) containing less than four buildings, (2) negligibly small (i.e., with an area of less than 0.1 km²), (3) with a shape factor (*SF*) larger than 0.1, or (4) exhibiting highly irregular shapes. This ensured the removal of blocks with uncommon geometry, with one or very few buildings, as well as removing huge industrial areas in the external neighborhoods of the city. The final population of urban blocks was then subjected to the calculation of ten quantitative urban metrics [35,36] (see Table 1 for their defining equations): Floor Area Ratio (*FAR*), Surface Coverage (*SC*), Volume Area Ratio (*VAR*), Green Ratio (*GR*), Relative Compactness (*REC*), Average Building Height (*ABH*), Shape Factor (*SF*), Vertical-to-Horizontal Ratio (*VtH*), Average Building Distance (*ABD*), and Sky View Factor (*SVF*).

Table 1. List of urban metrics.

Metric	Formula	Description of Inputs
Floor Area Ratio (<i>FAR</i>)	$FAR = \frac{\sum(A_i \cdot m_i)}{A_{\text{block}}}$	<i>A_i</i> : floor area of each <i>i</i> -th building in the block <i>A_{block}</i> : area of the block <i>m</i> : number of floors for each <i>i</i> building
Volume Area Ratio (<i>VAR</i>)	$VAR = \frac{\sum V_i}{A_{\text{block}}}$	<i>V_i</i> : volume of each <i>i</i> -th building in the block <i>A_{block}</i> : area of the block
Relative Compactness (<i>REC</i>)	$REC = \frac{\sum \frac{6V_i^{2/3}}{A_{i,\text{frontal}}}}{n}$	<i>V_i</i> : volume of each <i>i</i> -th building in the block <i>A_{i,frontal}</i> : area of the facades facing the streets of each <i>i</i> -th building <i>n</i> : number of buildings in the block
Shape Factor (<i>SF</i>)	$SF = \frac{A_{\text{block}}}{\pi r_{\text{min bounding}}^2}$	<i>A_{block}</i> : area of the block <i>r_{min bounding}</i> : radius of the minimum circle enclosing the block
Surface Coverage (<i>SC</i>)	$SC = \frac{\sum A_i}{A_{\text{block}}}$	<i>A_i</i> : footprint area of each <i>i</i> -th building in the block <i>A_{block}</i> : area of the block
Green Ratio (<i>GR</i>)	$GR = \frac{A_{\text{veg}}}{A_{\text{block}}}$	<i>A_{veg}</i> : green surface (trees, grass, etc.) in the block <i>A_{block}</i> : area of the block
Average Building Height (<i>ABH</i>)	$ABH = \frac{\sum h_i}{n}$	<i>h_i</i> : height of each <i>i</i> -th building in the block <i>n</i> : number of buildings in the block
Sky View Factor (<i>SVF</i>)	-	Calculated with a QGIS plugin
Average Building Distance (<i>ABD</i>)	$ABD = \frac{1}{n} \cdot \sum_i^n \left(\frac{\sum_{j \neq i}^n d_{ij}}{n-1} \right)$	<i>d_{ij}</i> : distance between <i>i</i> -th-building and <i>j</i> -th-building in the block <i>n</i> : number of buildings in the block
Vertical to Horizontal (<i>VtH</i>)	$VtH = \frac{\sum A_{\text{vert}}}{A_{\text{block}}}$	<i>A_{vert}</i> : vertical surfaces of the buildings <i>A_{block}</i> : area of the block

Next, a correlation analysis among these ten urban metrics, performed according to the Spearman test with a statistical significance $\alpha = 0.01$, was exploited to reduce the complexity of the dataset by identifying (and discarding) strongly interrelated metrics. When two metrics were found to be highly correlated (i.e., the absolute value of the Spearman $|\rho|$ was found larger than 0.5), the decision on which one to keep was made (1) after observing its correlation with the rest of the 10-metric set and (2) based on references from the literature on the most frequently used ones (e.g., Refs. [35,36]). Finally, in order to also account for the subsequent steps of the overall methodology (i.e., the modeling of weather files inclusive of UHI effects by means of the Urban Weather Generator, UWG), the final selection also accounted for those quantities underlined as particularly significant

in the UWG mathematical models [20,37]. At this stage, the statistical distributions of selected, uncorrelated urban metrics were characterized and used to perform stratified sampling at key summary points (10th percentile, first quartile, median, third quartile, and 90th percentile). The factorial combination of the extracted values of the selected urban metrics allowed us to define a smaller set of urban blocks, collectively representing the morphological variability of the study area.

In order to find urban blocks of particular interest for the assessment of the urban heat island phenomena, the next stage of the implemented procedure exploited land surface temperature data, *LST*, in agreement with consolidated practices from the literature (e.g., Refs. [38–41]). *LST* is often used as a proxy to identify hot spots with warmer air temperatures in the urban environment (e.g., Refs. [42,43]). Indeed, although *LST* clearly differs from the air temperature, which is one of the main inputs required in building performance simulation and urban building energy modeling, they are both positively correlated with solar radiation. Nevertheless, additional factors, such as the presence of green surfaces, can significantly alter this relationship. As a consequence, a preliminary comparison between ground-based weather station air temperature data and *LST* maps is recommended, in order to identify specific features in the urban texture (e.g., large green areas or rivers) that could introduce significant uncertainty in the procedure.

As a source of satellite *LST* imagery for this work, the ECOSTRESS (ECOSystem Spaceborne Thermal Radiometer Experiment on Space Station) data, made available by NASA [44], were considered. ECOSTRESS was selected since, up to date, it constitutes the dataset with the most detailed temperature images of the Earth's surface acquired from space. Focus was placed on the summer period and on days affected by heat wave phenomena. Also in this case, raw images were filtered in order to ensure an acceptable level of quality (i.e., excluding those with an excess of cloud cover or missing data, as well as those with the quality index provided by NASA lower than 0.75). A minimum set of twelve high-quality images was expected to be assembled to capture temporal and spatial variability; for each urban block, the mean *LST* was computed across the selected scenes to obtain a representative thermal signature.

The morphological and thermal imagery results were then merged so that from the pool of morphologically representative blocks, those exhibiting the highest average *LST* could be identified as priority archetypes (i.e., urban forms that are both typical of the city's-built environment and particularly relevant from a heat-stress perspective).

Finally, the use category and construction period served as the main criteria for assigning the corresponding building archetype features (i.e., typical construction and technical building systems) to the representative urban blocks, according to data available in the literature.

2.3. Current and Future Weather Data Incorporating UHI Effects

Rural climatic data were obtained from the nearest weather station, situated in a free-field area, selected as the closest rural location with at least ten years of continuous data. The dataset, which in Italy is usually made available through the Regional Environmental Protection Agency (ARPA), was used to generate the typical meteorological year (TMY) representing current climate conditions. Subsequently, the mid- and long-term future weather files were created in accordance with the IEA-EBC Annex 80 Weather Data Task Group methodology [45].

The generation of the current, mid-, and long-term urban weather files was performed using the Urban Weather Generator (UWG) [20,37], based on 3D models of the selected urban blocks. These models include geometric and physical parameters representative of both the urban morphology and the corresponding building archetypes.

2.4. Key Performance Indicators

This section defines the KPIs adopted to quantify the intensity, frequency, and sensitivity of the urban warming effect under different climate change scenarios. Table 2 summarizes the selected metrics, encompassing both building energy performance, indoor thermal comfort, and climate-related indicators, along with their symbol, terminology, units, and corresponding references.

The thermal energy needs for space heating and cooling ($EP_{H/C,nd}$) were selected to assess the building stock energy performance across climate pathways. Moreover, the hourly heating and cooling load peaks ($\Phi_{H/C,ld}$) over the calculation period are relevant for sizing technical building systems. These indicators can be calculated directly from any UBEM tool.

Indoor thermal comfort KPIs are dependent on operative temperature and are generally computed for representative spaces, where zoning discretization is particularly challenging in UBEM applications. In large-scale energy analyses, buildings are typically modeled as a single-thermal zone, although some UBEM tools incorporate auto-zoning algorithms. For instance, umi [46] applied a clustering method to generate shoebox energy models based on solar radiation received by façades [47]. In addition, several UBEM tools compute the indoor air temperature instead of internal operative temperature.

The weighted warm hours of discomfort (WHD_w) can be calculated in free-floating according to EN ISO 7730 [48] or CEN/TR 16798-2 [49]. The former emphasizes the intensity of thermal discomfort, whereas the latter reflects the magnitude of temperature exceedance under adaptive comfort conditions. The indoor overheating degree (IOD) and overheating escalation factor (α_{IOD}), introduced by [50], further quantify the risk of indoor overheating by considering both the severity and frequency of excessive temperatures. The IOD measures the temperature difference between the free-running indoor operative temperature and the selected thermal comfort limit, while the frequency is derived by integrating the overheating intensity over the occupied period. The α_{IOD} , calculated as the ratio between IOD and ambient warmness degree (AWD), indicates the building's sensitivity to overheating. Assuming a linear relationship between IOD and AWD , α_{IOD} corresponds to the slope of the regression line.

Climate-related KPIs are directly dependent on outdoor temperature. The ambient warmness degree (AWD), as defined in [50], quantifies the severity and duration of high outdoor temperatures relative to a predefined base temperature, typically 18 °C, which represents the lower comfort threshold during the heating season. As reported in Equation (1), only positive differences between the i -th hourly external air temperature ($\theta_{e,i}$, in °C) and the base temperature (θ_b , in °C) are considered in the summation and normalised to the total number of occupied hours (N) in the building.

$$AWD = \frac{\sum_{i=1}^N (\theta_{e,i} - \theta_b)^+ t_i}{\sum_{i=1}^N t_i} \quad (1)$$

The heating degree days (HDD) and cooling degree days (CDD) are synthetic indicators describing how warm or cold a territory is over a given period.

Table 2. List of KPIs in different fields.

Quantity	Symbol	Unit	Ref.
Energy Performance			
Energy need for space heating per unit conditioned floor area	$EP_{H,nd}$	$\text{kWh}\cdot\text{m}^{-2}$	[51,52]
Energy need for space cooling per unit conditioned floor area	$EP_{C,nd}$	$\text{kWh}\cdot\text{m}^{-2}$	[51,52]
Peak heating load per unit conditioned floor area	$\Phi_{H,ld}$	$\text{W}\cdot\text{m}^{-2}$	[51,52]
Peak cooling load per unit conditioned floor area	$\Phi_{C,ld}$	$\text{W}\cdot\text{m}^{-2}$	[51,52]
Indoor Thermal Comfort			
Weighted Warm Hours of Discomfort	WHD_w	h	[48,53]
Indoor Overheating Degree	IOD	$^{\circ}\text{C}$	[50]
Overheating Escalation Factor	α_{IOD}	-	[50]
Climate			
Ambient Warmness Degree	AWD	$^{\circ}\text{C}$	[50]
Heating Degree Days	HDD	$^{\circ}\text{C}\cdot\text{d}$	[54]
Cooling Degree Days	CDD	$^{\circ}\text{C}\cdot\text{d}$	[54]
Urban Heat Island Intensity	$UHII$	$^{\circ}\text{C}$	[55]

Finally, the urban heat island intensity ($UHII$) represents the temperature difference between an urban weather station (UWS) and a rural weather station (RWS). This metric can be computed using either the average monthly temperature difference between UWS and RWS [55], or the monthly maximum and minimum external air temperature at the two weather stations [7]. The first approach is expressed in Equation (2), where $UHII_m$ is calculated for the m -th month. In this formula, $\bar{\theta}_{e,UWS;h;m}$ (in $^{\circ}\text{C}$) denotes the average monthly external air temperature recorded at the urban station, while $\bar{\theta}_{e,RWS;h;m}$ (in $^{\circ}\text{C}$) refers to that recorded at the RWS.

$$UHII_m = \bar{\theta}_{e,UWS;h;m} - \bar{\theta}_{e,RWS;h;m} \quad (2)$$

In this work, the performance of the representative urban blocks of Turin was assessed using the indicators reported in Table 2 that relate to energy performance and climate-related metrics. From this perspective, indoor thermal comfort KPIs were not considered, as in UBEMs, buildings are typically represented as single thermal zones. This modeling assumption limits the ability to reliably capture the spatial variability of indoor conditions and the subdivision of internal spaces through vertical and/or horizontal partitions.

3. Application

3.1. Analysis of Urban Metrics and Satellite Images for Turin

Starting with a comprehensive dataset of the building cadastral parcels, all buildings in Turin, more than 128,000, were aggregated into 4,518 urban blocks and then reduced to 2804 urban blocks thanks to the screening activity presented in Section 2.2. For each of them, the selected ten urban metrics were computed. By means of the Spearman correlation analysis (Table 3), which was used to identify and remove redundant indicators, this set was reduced to four key urban metrics: Surface Coverage (SC), Green Ratio (GR), Average

Building Height (*ABH*), and the Vertical-to-Horizontal ratio (*VtH*). Further details on the correlation procedure and the statistical distributions of the retained metrics are reported in Borelli et al. [34]. Sampling these distributions for *SC*, *GR*, *ABH*, and *VtH* produced a preliminary pool of 171 representative urban blocks for the city of Turin that were able to capture the main morphological features of its building stock.

Table 3. Spearman correlation analysis: in light red $|\rho| > 0.5$, in dark red unitary correlation.

<i>FAR</i>	1									
<i>VAR</i>	0.85	1								
<i>REC</i>	−0.40	−0.51	1							
<i>SF</i>	0.06	0.06	−0.02	1						
<i>SC</i>	0.54	0.61	0.01	0.06	1					
<i>GR</i>	−0.27	−0.30	0.13	−0.04	−0.37	1				
<i>ABH</i>	0.60	0.73	−0.71	0.06	0.08	−0.10	1			
<i>SVF</i>	−0.26	−0.29	0.32	−0.10	−0.17	0.20	−0.25	1		
<i>ABD</i>	−0.16	−0.13	0.22	−0.21	−0.03	0.50	−0.08	0.27	1	
<i>VtH</i>	0.63	0.64	−0.53	0.24	0.19	−0.34	0.61	−0.34	−0.59	1
	<i>FAR</i>	<i>VAR</i>	<i>REC</i>	<i>SF</i>	<i>SC</i>	<i>GR</i>	<i>ABH</i>	<i>SVF</i>	<i>ABD</i>	<i>VtH</i>

Eighteen land surface temperature (*LST*) images from summer 2023 were analyzed to guide the selection of the most relevant blocks for the UBEEM simulations. Figure 1 shows one of the processed *LST* satellite maps as an example. For the whole city, the average *LST* for each block from the available imagery was computed, providing a comprehensive characterization of the impact of the UHI across the study area. As shown in Figure 2a, which depicts the average *LST*s of the different urban blocks of Turin for the analyzed set of thermal images, the observed *LST*s ranged from 22 °C in the rural area southeast of the Po River up to 31.7 °C in industrial neighborhoods.

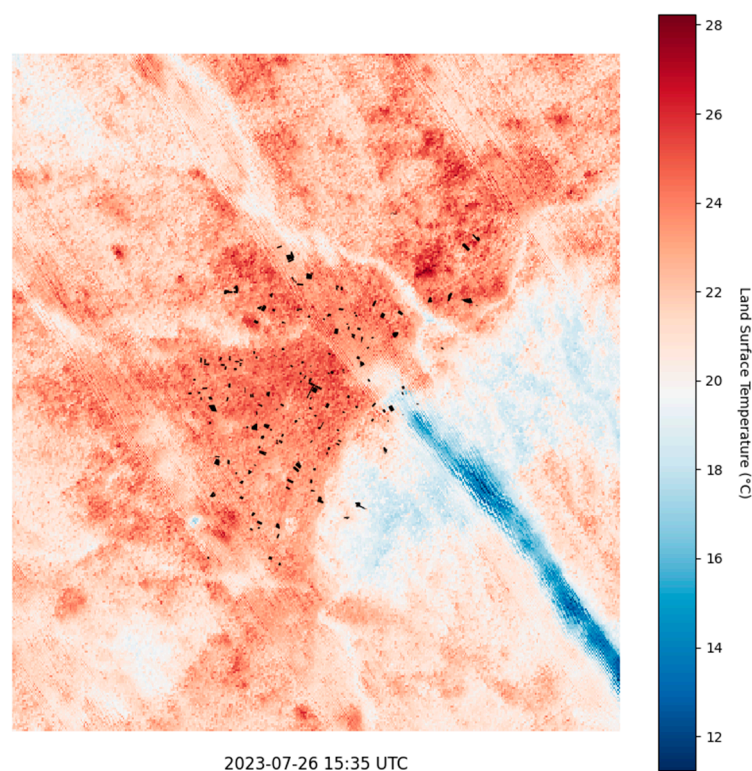
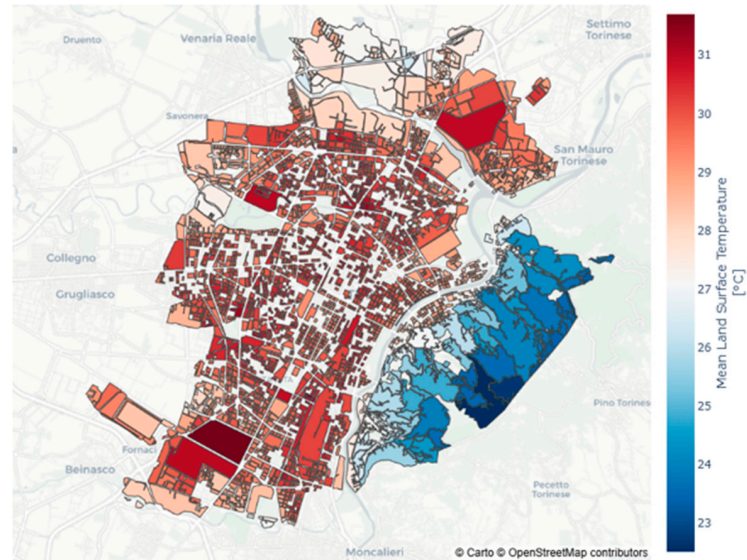
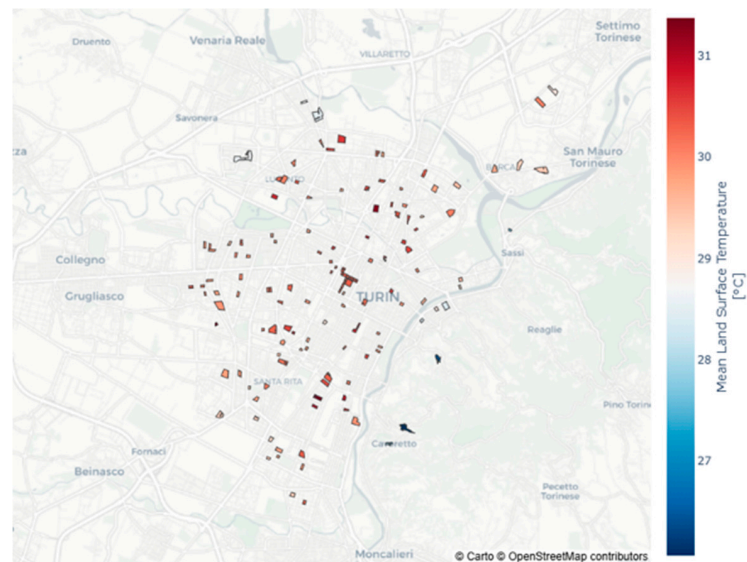


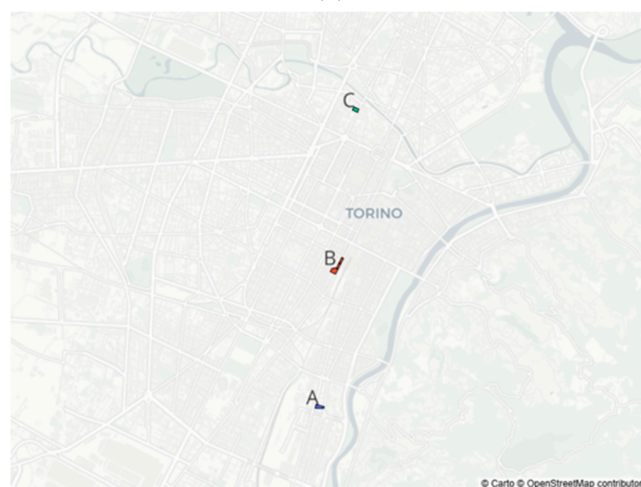
Figure 1. Example of processed ECOSTRESS satellite map of land surface temperature for Turin on 26 July 2023. Black polygons highlight the representative urban blocks selected through the morphology analysis.



(a)



(b)



(c)

Figure 2. Maps of the average land surface temperatures for each urban block, obtained by analyzing 18 satellite maps from summer 2023: representation of the mean *LST* for the whole city (partially revised from [56]) (a), for the representative urban blocks (b), and position of the three selected urban blocks A, B, and C (c). Maps developed starting from OpenStreetMap [57].

By combining the morphological sampling with the *LST*-based screening, the candidate set was narrowed to 130 blocks, the reduction being due to missing or insufficiently accurate satellite data for some of the initially selected blocks. This final subset exhibited average *LST* values between 25.0 °C and 31.4 °C (Figure 2b). Figure 2c highlights the three blocks with the highest *LST*s (i.e., blocks A, B, and C), with average land surface temperature values of 30.6 °C, 30.7 °C, and 30.9 °C, respectively. These three urban blocks were considered among those as the most affected by local microclimatic alteration from the UHI effect, and thus representative for the subsequent simulative analyses part of this research.

3.2. Urban Archetypes

The building use categories, construction periods, footprints, and heights of urban blocks A, B, and C, represented in Figure 3, were retrieved from the Geoportal of the Metropolitan City of Turin [58]. The geometrical building data were converted into a GeoPackage format, distinguishing thermally simulated zones from shading objects (i.e., adjacent constructions) and incorporating equilateral triangular ground meshes. These GeoPackage files were subsequently imported into CitySim [59] for urban-scale energy performance simulations.

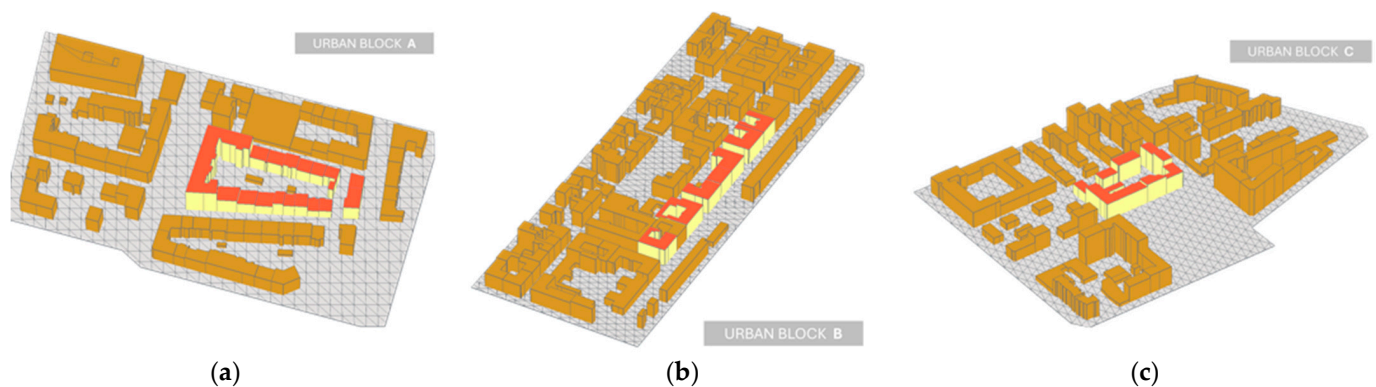


Figure 3. Representative urban blocks A (a), B (b), and C (c) of Turin, visualized in CitySim Pro.

Table 4 reports the main general and geometric urban metrics for urban blocks A, B, and C. Specifically, the selected metrics included the number of thermally assessed buildings, surface coverage (*SC*), average building height (*ABH*), compactness ratio ($A_{env} \cdot V^{-1}$), and green ratio (*GR*). Urban block C exhibited the highest median compactness ratio, which is expected to influence the calculation of heat transfer through the building envelope. Conversely, urban block B was characterized by buildings with greater vertical development and by the highest degree of urbanization, as indicated by its *SC* value.

Table 4. Relevant urban metrics for urban blocks A, B, and C.

Parameter	Unit	Urban Block		
		A	B	C
No. of assessed buildings	-	17	8	9
Surface Coverage, <i>SC</i>	-	0.322	0.388	0.323
Average Building Height, <i>ABH</i>	m	18.8	20.5	17.4
Compactness Ratio (median), $A_{env} \cdot V^{-1}$	m^{-1}	0.300	0.251	0.316
Green Ratio, <i>GR</i>	-	0.00	0.00	0.07

Taken as an example, the 3D geometric model of urban block A is illustrated in Figure 4, highlighting the associated building codes. Located in the southern part of the municipality of Turin, block A comprises seventeen thermally simulated residential buildings, mostly constructed between 1921 and 1945.



Figure 4. Representative urban block A of Turin, visualized in CitySim Pro.

For urban block A, Table 5 reports both the geometrical and thermophysical characteristics of the assessed buildings. In particular, these parameters include building floor area (A_{fl}), total thermal envelope area (A_{env}), volume (V), window-to-wall ratio (WWR), compactness ratio ($A_{env} \cdot V^{-1}$), and mean thermal transmittance for opaque (U_{op}) and transparent (U_{wi}) components.

The use category and construction period served as the main criteria for assigning the corresponding building archetypes. Specifically, the thermal properties of opaque and transparent envelope components were derived from archetype schemas developed within the PRIN2020 URBEM (Urban Reference Buildings for Energy Modeling) [16] and the H2020 TIMEPAC (Towards Innovative Methods for Energy Performance Assessment and Certification of Buildings) projects [60]. Moreover, the internal heat gain schedules and intensities—including occupants, appliances, and lighting—were taken from the Italian National Annex of UNI EN 16798-1 [61]. Furthermore, for all the assessed buildings, the ventilation air change rate was assumed to be 0.5 h^{-1} , while the winter and summer indoor temperature set-points were set at $20 \text{ }^\circ\text{C}$ and $26 \text{ }^\circ\text{C}$, respectively.

Table 5. Geometrical and mean thermal characteristics for opaque and transparent components in representative urban block A.

Bldg. Code	Constr. Period	A_{fl} [m ²]	A_{env} [m ²]	V [m ³]	WWR [-]	$A_{env} \cdot V^{-1}$ [m ⁻¹]	U_{op} [W·m ⁻² ·K ⁻¹]	U_{wi} [W·m ⁻² ·K ⁻¹]
A_1	1921–45	524	648	1917	14%	0.338	1.45	3.09
A_2		776	1357	2654		0.511	1.42	
A_3		371	671	1508		0.445	1.47	
A_4		748	1045	2860		0.365	1.47	
A_5		639	743	2364		0.314	1.46	
A_6		13,200	11,126	45,540		0.244	1.43	
A_7		1387	1315	5086		0.258	1.46	
A_8		877	954	3244		0.294	1.47	
A_9		849	880	2943		0.299	1.45	
A_10		980	949	3409		0.278	1.48	
A_11		875	937	3227		0.290	1.47	
A_12		689	707	2480		0.285	1.48	
A_13		775	868	2964		0.293	1.49	
A_14		665	713	2380		0.300	1.47	
A_15		351	480	1321		0.363	1.51	
A_16	1946–60	587	661	2085	13%	0.317	1.28	3.12
A_17		1401	1680	5044		0.333	1.27	

3.3. Current and Future Weather Data for the Urban Archetypes

To ensure a consistent basis for the generation of current and future climate scenarios, weather data were extracted from regional climate model outputs, in accordance with the IEA-EBC Annex 80 Weather Data Task Group methodology [45]. The rural climatic data were extracted for the weather station located in Turin Bauducchi, situated in a free-field area (latitude 44.96° N, longitude 7.70° E, and altitude 226 m a.s.l.). This station, approximately 9 km from urban block A, was selected as the closest rural location.

The observational dataset, sourced from ARPA Piemonte (Regional Environmental Protection Agency) [62] and covering ten years of continuous data (1994–2003), was used as reference data for the calibration and bias-correction procedure applied to the regional climate model. Finally, the typical meteorological year (TMY) representing current climate conditions (2013–2023), as well as the mid-term (2041–2060) and long-term (2081–2100) future weather files, were generated from the bias-corrected outputs.

The generation of the current, mid-, and long-term urban weather files was performed using UWG [20,37] based on 3D models of the selected urban blocks. For the generation of urban weather files, besides the geometrical, optical, and thermophysical properties of buildings, attention was given to green cover (Table 4) and the surface albedo. Specifically, the green cover was 0.07 for block C and null for the other two blocks; albedo values of roads, vegetation, roofs, and walls were 0.10, 0.26, 0.40, and 0.70, respectively. The glazing ratio of the facades ranged from 0.13 to 0.15; for the windows, a $SGHC$ of 0.675 was assigned. Regarding the anthropogenic heat, preliminary sensitivity analyses proved that this variable had a negligible impact for the tested urban; since this input was not available, the standard value of 4 W/m² reported by UWG for some examined cities was consequently adopted.

4. Results and Discussion

4.1. Climate-Related KPIs Assessment

Taking urban block A as an example, the heating and cooling degree days—computed for a base temperature of 18 °C, respectively, HDD_{18} and CDD_{18} —according to UNI 10349-3 [63] for both the RWS and UWS under current, mid-, and long-term scenarios, are reported in Figure 5. The results indicate a 15–23% reduction in $HDDs$ and a 25–33% increase in $CDDs$ in urban compared to rural contexts, confirming a more pronounced and persistent urban effect during summer. Table 6 reports the percentage variations in HDD_{18} and CDD_{18} between current and future urban conditions. The findings highlight a dramatic increase of 87.7% in CDD_{18} under the long-term scenario, accompanied by a 33.9% decrease in HDD_{18} . In the mid-term scenario, the variations are less pronounced, with a 9.2% reduction in HDD_{18} and a 27.6% increase in CDD_{18} relative to current conditions.

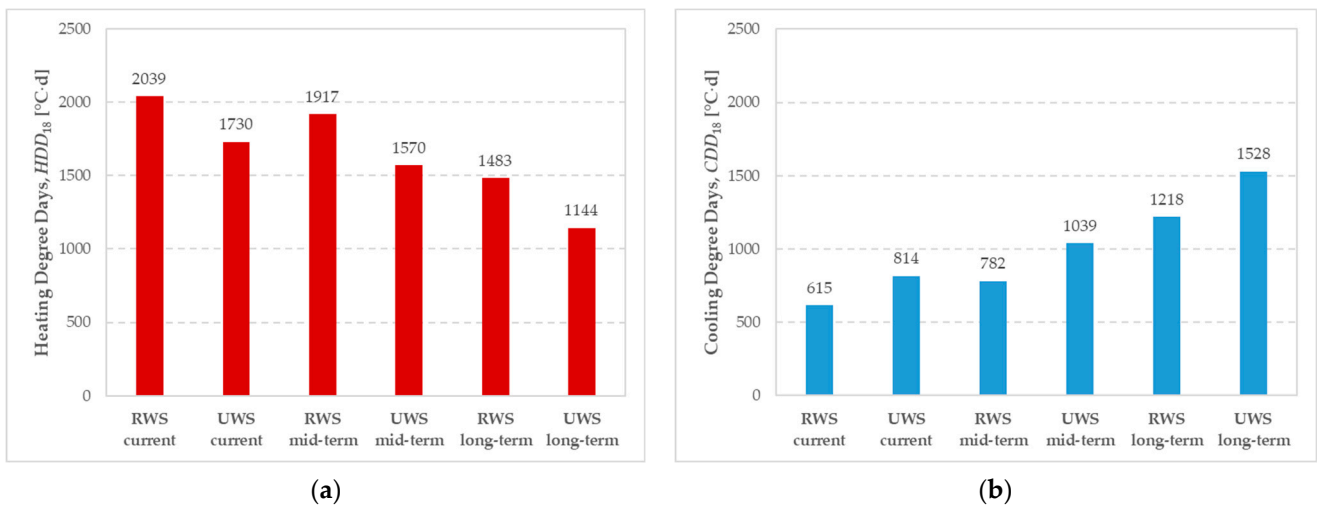


Figure 5. Heating degree days (a) and cooling degree days (b) based on RWS and UWS data for the current, mid-, and long-term periods in urban block A.

Figure 6 presents the ambient warmness degree calculated with a reference temperature of 18 °C (AWD_{18}) and the urban heat island intensity ($UHII$) under different climate conditions for urban block A, as defined by Equations (1) and (2), respectively. The AWD_{18} was calculated over the summer period (June August).

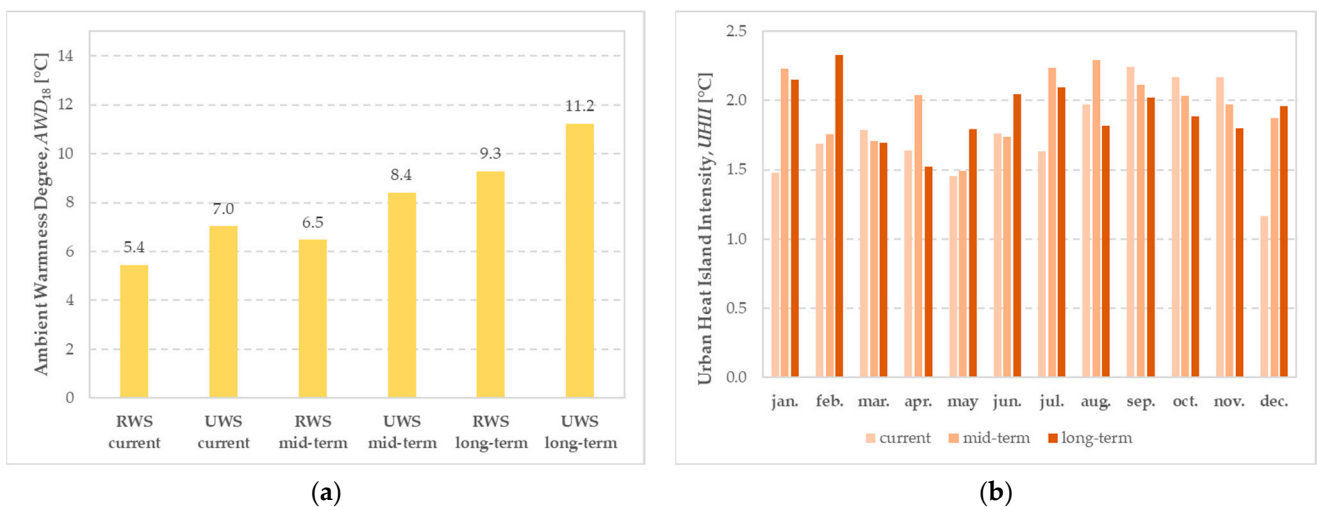


Figure 6. Ambient warmness degree (a) and urban heat island intensity (b) based on RWS and UWS data for the current, mid-, and long-term periods in urban block A.

Under current conditions, AWD_{18} reached 5.4 °C at the rural site and 7.0 °C in the urban area, confirming a warmer urban microclimate. In the mid-term scenario, both stations exhibited a further increase, up to 6.5 °C (RWS) and 8.4 °C (UWS). The long-term scenario revealed a substantial intensification of warm conditions, with AWD_{18} values of 9.3 °C for RWS and 11.2 °C for UWS. The latter indicates that, on average, the external air temperature exceeded the 18 °C threshold by more than 11 °C during the analyzed warm period.

Table 6 reports the percentage variation of AWD_{18} at the UWS relative to the current scenario. A notable increase of approximately 60% was observed under the long-term scenario, corresponding to an average rise of about 4.2 °C in outdoor temperature.

Table 6. Variation in HDD_{18} , CDD_{18} , and AWD_{18} based on UWS data, relative to the current scenario.

Scenarios	ΔHDD_{18} [°C·d]	ΔCDD_{18} [°C·d]	ΔAWD_{18} [°C]	ΔHDD_{18} [-]	ΔCDD_{18} [-]	ΔAWD_{18} [-]
Mid-term—current	−160	+225	+1.4	−9.2%	+27.6%	+19.7%
Long-term—current	−586	+714	+4.2	−33.9%	+87.7%	+59.7%

Overall, the $UHII$ (Figure 6b) remained positive throughout the year, confirming the consistent presence of the urban heat island effect across all seasons and climatic conditions. The monthly average $UHII$ values ranged between 1.5 and 2.3 °C, reflecting the thermal inertia of the urbanized area.

4.2. KPIs Assessment of Urban Block A

The weather files derived from the UWG tool were used as input for the CitySim models to assess the impact of the microclimate variations. For each representative urban block, the analysis focused on the calculation of both thermal energy needs for space heating and cooling ($EP_{H/C,nd}$) and the peak heating/cooling load ($\Phi_{H/C,ld}$).

The fluctuations in building energy need, which are strongly influenced by variations in external air temperature, are more pronounced than those in peak heating/cooling loads. The latter depends not only on air temperature but also on solar irradiance and building inertia.

Figure 7 illustrates the thermal energy need for space heating (a) and cooling (b) across different buildings (A_1–A_17) under current, mid-term, and long-term UWS climatic conditions. The assessed buildings are residential apartment blocks predominantly built from 1921 to 45 within urban block A. Overall, the results highlight a progressive shift in building energy need profiles—from heating-dominated to cooling-dominated conditions—emphasizing the need for adaptive design strategies aimed at improving summer comfort and reducing future cooling loads. Buildings A_2 and A_3 experienced the highest thermal energy need for space heating and cooling, approximately 100 kWh/m² and 33–38 kWh/m², respectively, under long-term UWS conditions. These buildings also presented the highest compactness ratio ($A_{env} \cdot V^{-1}$) within the assessed urban context. Conversely, apartment block A_6 showed the lowest energy need, with an $EP_{H,nd}$ of 51.5 kWh/m² and $EP_{C,nd}$ of 22.8 kWh/m². A similar trend can be observed in Figure 8, which presents the peak heating (a) and cooling (b) loads.

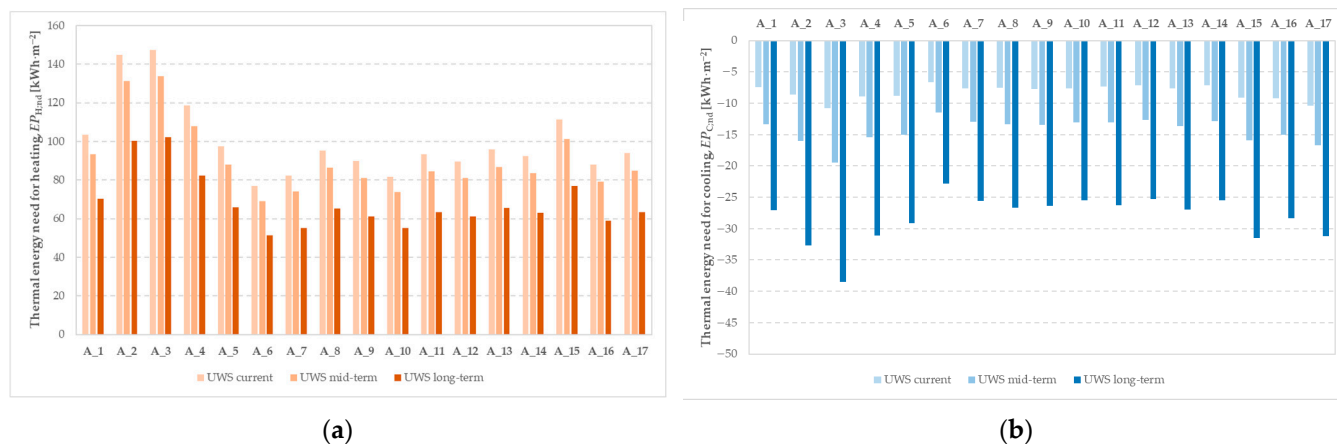


Figure 7. Thermal energy need for space heating (a) and cooling (b) using UWS data for the current, mid-, and long-term periods.

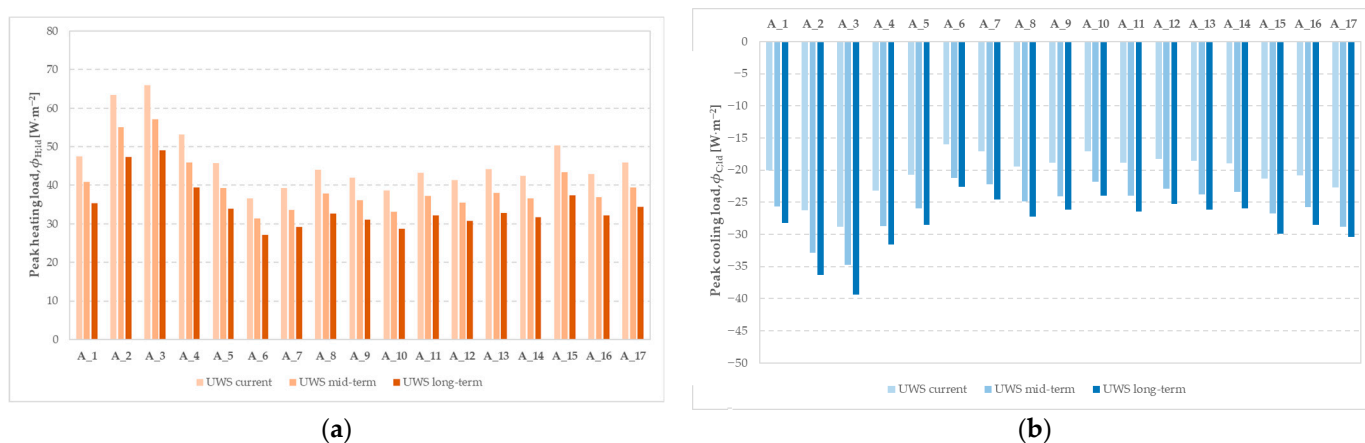


Figure 8. Peak heating (a) and cooling (b) loads using UWS data for the current, mid-, and long-term periods.

The results highlight how building geometry, solar gains, and the thermophysical properties of building archetypes jointly influence overall energy performance. This analysis underscores the relevance of correcting climate variables when assessing the future energy need of buildings.

4.3. KPIs Assessment of the Urban Archetypes

This section presents the aggregated results for the three selected representative urban blocks of the municipality of Turin, highlighting the differences in energy performance within the same urban context. Specifically, Figure 9a–c reports the thermal energy need for space heating and cooling—calculated as the net floor area-weighted average of the buildings in urban blocks A, B, and C, respectively—using UWS climate data under three different climate periods.

Several driving factors influence the energy intensity at the city-block scale. First, the geometry of the buildings within the UBEM domain affects the magnitude of heat transfer through both opaque and transparent envelope components. Second, the non-geometric characteristics defined in the building archetype schema—particularly those related to the construction period—affect the building typology and thermal properties of envelope elements. Finally, the morphological configuration of each block, including shading patterns and façade orientation, determines the contribution of solar heat gains.

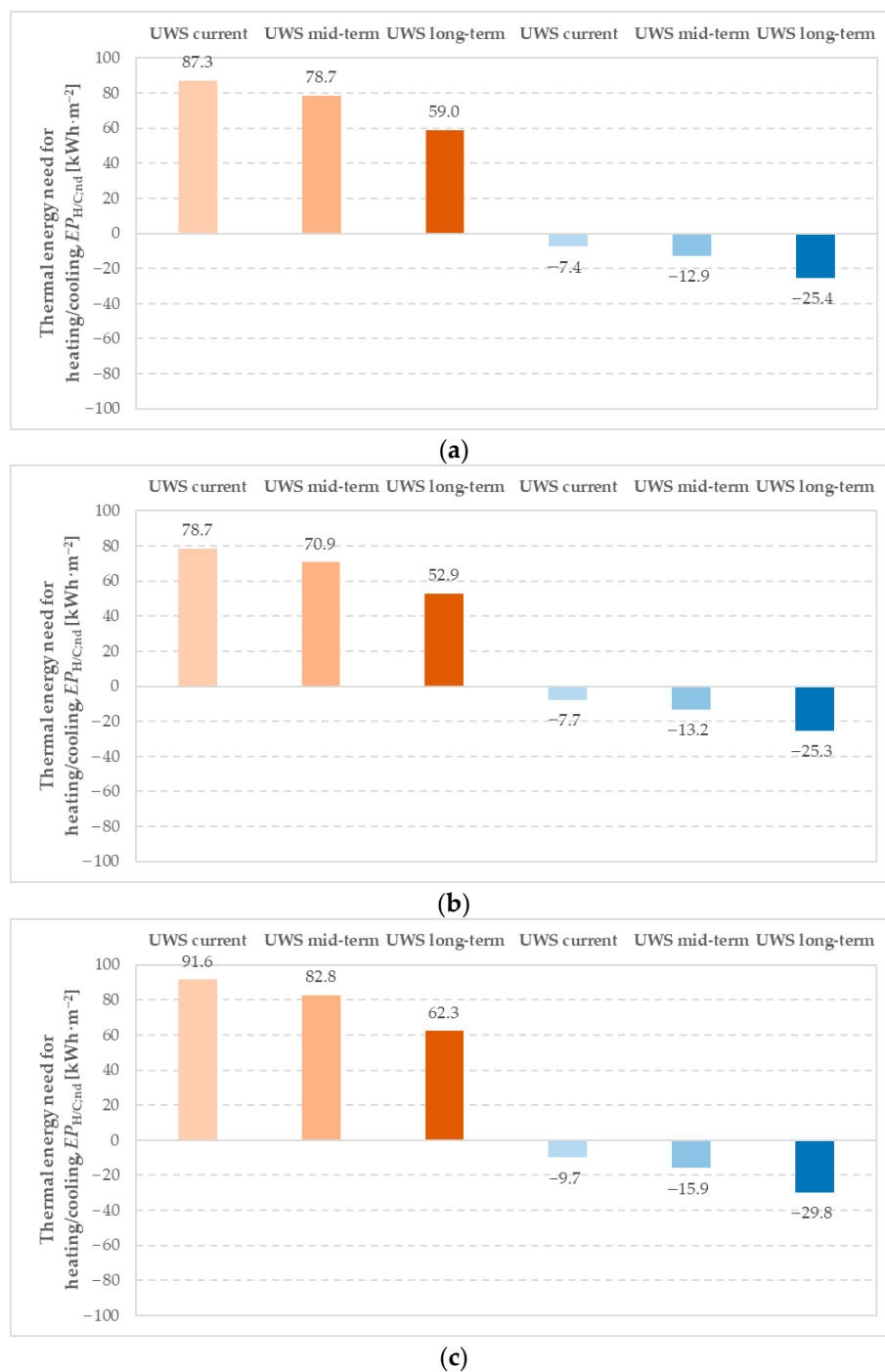


Figure 9. Thermal energy need for space heating (positive bars) and cooling (negative bars) for urban blocks A (a), B (b), and C (c) using UWS data for the current, mid-, and long-term periods.

Overall, the geometry and morphological characteristics of the urban blocks emerged as factors governing the variation in thermal energy needs for both heating and cooling.

The compactness ratio ($A_{env} \cdot V^{-1}$) affects the thermal energy need for space heating. As shown in Table 4, urban block C exhibited the highest $A_{env} \cdot V^{-1}$, followed by blocks A and B, resulting in the highest transmission heat losses through envelope components. A similar trend was observed for $EP_{H,nd}$ in the long-term scenario, with values of 62.3 kWh/m² for block C, 59.3 kWh/m² for block A, and 52.9 kWh/m² for block B.

Conversely, the effect on space cooling was less straightforward. A higher compactness ratio implies a greater surface area exposed to solar radiation, potentially increasing

cooling needs. In the long-term scenario, urban block C recorded the highest $EP_{C,nd}$ at 29.8 kWh/m², while both blocks A and B showed similar values of 25.3 kWh/m².

Table 7 presents the overall variation in urban block $EP_{H/C,nd}$ relative to the current scenario for case studies A, B, and C. In the mid-term, the reduction in heating need ranges between −9.6% and −10.0%, while the cooling need rises by 63.9% to 74.3%. The long-term scenario amplifies these trends, with the heating need decreasing by more than 30% and the cooling need more than doubling (+207.2% to +243.2%). This substantial rise in cooling energy need highlights the growing impact of warmer outdoor conditions and the increasing importance of summer thermal comfort in future climate contexts.

Table 7. Overall variation in urban block $EP_{H/C,nd}$ relative to the current scenario for case studies A, B, and C.

Scenarios	$\Delta EP_{H,nd}$ [kWh·m ^{−2}]	$\Delta EP_{C,nd}$ [kWh·m ^{−2}]	$\Delta EP_{H,nd}$ [-]	$\Delta EP_{C,nd}$ [-]
Urban block A				
Mid-term—current	−8.6	+5.5	−9.8%	+74.3%
Long-term—current	−28.3	+18.0	−32.4%	+243.2%
Urban block B				
Mid-term—current	−7.8	+5.5	−9.9%	+71.4%
Long-term—current	−25.8	+17.6	−32.7%	+228.6%
Urban block C				
Mid-term—current	−8.8	+6.2	−9.6%	+63.9%
Long-term—current	−29.3	+20.1	−32.0%	+207.2%

A linear correlation between building geometry and the building energy need can be observed in Figure 10. Specifically, the compactness ratio is shown as a function of the thermal energy need for space heating, considering all buildings belonging to urban blocks A, B, and C, under current-period UWS data. As discussed above, Figure 10 analytically illustrates the influence of building morphology on the space-heating energy need reported in Figure 9.

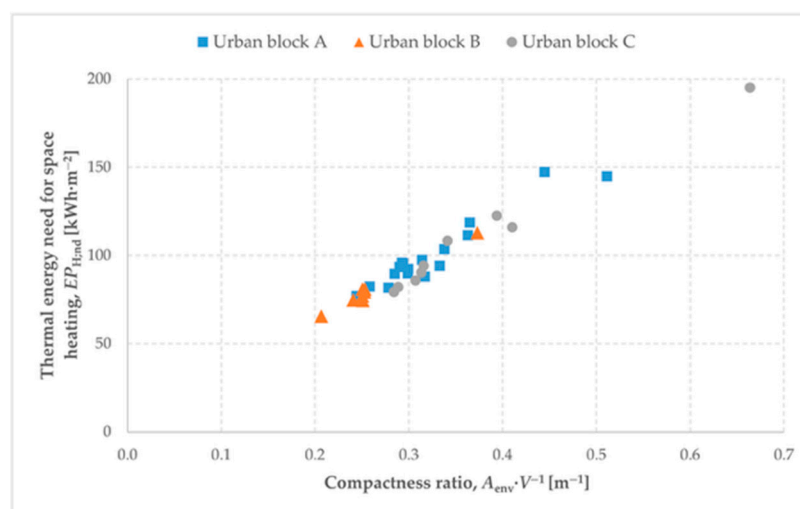


Figure 10. Linear correlation between the compactness ratio ($A_{env} \cdot V^{-1}$) and the thermal energy need for the space heating ($EP_{H,nd}$) of buildings within the three assessed urban blocks, based on UWS data for the current period.

5. Conclusions

Climate change and urban heat island effects are driving rising urban temperatures, significantly influencing building energy demand and indoor comfort. The PRIN2022-PNRR CRiStAll (Climate Resilient Strategies by Archetype-based Urban Energy Modeling) project developed detailed urban climate models and archetype-based energy analyses, relying on the representativeness of urban contexts under current and future climate scenarios. The innovation of this approach lies primarily in the data-driven selection of representative urban blocks through quantitative geometry-based metrics and statistical techniques applied to the entire urban fabric, and in their subsequent prioritization to identify urban forms that are both geometrically representative and vulnerable to UHI effects.

The CRiStAll project methodology, designed to assess the behavior of different city blocks under various greenhouse gases pathways, was presented in the article and applied to the case of Turin, a city located in northwestern Italy. The typical geometrical definition was based on relevant urban metrics, while ECOSTRESS NASA satellite images were employed to identify the areas of Turin most exposed to UHI effects, characterized by the highest summer surface temperatures. The selected representative urban blocks were subsequently modeled in the CitySim environment, with an appropriate set of non-geometric properties assigned and encapsulated within the building archetype schema. To capture microclimatic variations in urbanized contexts, the external air temperature and humidity ratio of the typical meteorological year (TMY) for the rural weather station—under current, mid-term, and long-term scenarios—were corrected using the Urban Weather Generator tool.

The assessed metrics were categorized into climate-dependent variables and energy performance indicators. Specifically, heating and cooling degree days (HDD_{18} and CDD_{18}), ambient warmth degree (AWD_{18}), and urban heat island intensity ($UHII$) were considered, along with the thermal energy need for space heating and cooling ($EP_{H/C,nd}$) and with the peak heating/cooling loads ($\Phi_{H/C,ld}$). Results were presented both disaggregated for a single urban block—taken as an example—and aggregated for three representative urban blocks selected.

Energy intensity at the city-block scale is influenced by multiple factors, including building geometry, construction-related thermal properties, and the morphological configuration of the urban fabric. Among these, geometry and morphology emerged as the dominant drivers of variations in thermal energy needs for heating and cooling. For the analyzed urban blocks, under the long-term scenario and compared to current conditions, the heating need decreases by more than 30% while the cooling need more than doubles (+207.2% to +243.2%). These findings highlight the growing influence of warmer climates and the critical importance of addressing summer thermal comfort in future urban contexts.

Future work will aim to apply the proposed methodology across different climatic zones and verify its applicability in municipalities characterized by heterogeneous and fragmented datasets. Further research will focus on expanding the number of KPIs, including metrics for outdoor thermal comfort assessment. Moreover, by developing a further research line within the CRiStAll framework, future research will implement grey, blue, and green mitigation strategies at the urban archetype level to quantify potential improvements in building stock energy performance and thermal comfort at the urban scale.

By adopting the urban archetype concept, the devised methodology can be applied to develop a *bottom-up* urban building energy model to assess KPIs for an entire city, scaling-up the urban archetype KPIs. To this purpose, a proper number of urban blocks should be selected to adequately represent the broader morphological variability of a city. By increasing the sample size of the archetypes, the UBEM would guarantee a wider spatial coverage of the outcomes and benefit from generalizable results.

Finally, performing a model calibration would be desirable. However, the available measured weather data are typically characterized by distances in the range of kilometers and are therefore unsuitable for validating the simulated UHI intensity at the micro-scale (city-block level). If measured data at the micro-scale (canopy layer) are acquired in the future, a comparison with simulated microclimatic data will be carried out.

The methodology and outcomes of the present research provide a practical and effective tool for policymakers and public administrations to promote urban renovation processes and facilitate the transition toward climate-resilient cities.

Author Contributions: Conceptualization, I.B., V.C., G.P. and A.G.; Formal analysis, M.P., M.P.T. and G.B.; Funding acquisition, I.B. and G.P.; Investigation, M.P., M.P.T. and G.B.; Methodology, M.P., I.B., M.P.T., V.C., G.P., G.B. and A.G.; Project administration, I.B.; Software M.P., M.P.T. and G.B.; Supervision, V.C. and A.G.; Validation, M.P., I.B., M.P.T., G.P. and G.B.; Visualization, M.P.; Writing—original draft, M.P., I.B., M.P.T., G.P. and G.B.; Writing—review and editing, M.P., I.B., M.P.T., V.C., G.P., G.B. and A.G. All authors have read and agreed to the published version of the manuscript.

Funding: This study was carried out within the «Climate Resilient Strategies by Archetype-based Urban Energy Modeling (CRiStAll)» project—funded by European Union—Next Generation EU within the PRIN 2022 PNRR program (D.D.1409 of 14/09/2022 Ministero dell’Università e della Ricerca), M4C2, I 1.1. Part of this was developed in the framework of the PhD Research Scholarship “Development of urban building energy models to support the definition of energy policies by municipalities and local public administrations” (DM 118/2023). This manuscript reflects only the authors’ views and opinions and the Ministry cannot be considered responsible for them.

Data Availability Statement: The original contributions presented in this study are included in the article. Further inquiries can be directed to the corresponding author.

Conflicts of Interest: The authors declare no conflicts of interest.

Nomenclature

Quantities

<i>A</i>	Area (m ²)
<i>ABD</i>	Average building distance (m)
<i>ABH</i>	Average building height (m)
<i>AWD</i>	Ambient warmness degree (°C)
<i>CDD</i>	Cooling degree days (°C·d)
<i>EP</i>	Energy performance (kWh·m ⁻²)
<i>FAR</i>	Floor area ratio (-)
<i>GR</i>	Green ratio (-)
<i>HDD</i>	Heating degree days (°C·d)
<i>IOD</i>	Indoor overheating degree (°C)
<i>LST</i>	Land surface temperature (°C)
<i>REC</i>	Relative compactness (-)
<i>SC</i>	Surface coverage (-)
<i>SF</i>	Shape factor (m ⁻¹)
<i>SVF</i>	Sky view factor (-)
<i>U</i>	Thermal transmittance (W·m ⁻² ·K ⁻¹)
<i>UHII</i>	Urban heat island intensity (°C)
<i>V</i>	Volume (m ³)
<i>VAR</i>	Volume to area ratio (m)
<i>VtH</i>	Vertical to horizontal ratio (-)
<i>WDH</i>	Weighted hours of discomfort (h)
<i>WWR</i>	Window-to-wall ratio (-)

Greek symbols

α	Overheating escalation factor (-)
θ	Temperature ($^{\circ}\text{C}$)
Φ	Areic heat load ($\text{W}\cdot\text{m}^{-2}$)

Subscripts

a	Air
avg	Average
C	Cooling
e	External, outdoor
env	Envelope
fl	Floor
H	Heating
ld	Load
m	Monthly
nd	Need
op	Opaque (envelope)
w	Warm
wi	Window

Acronyms

IPCC	Intergovernmental Panel on Climate Change
KPI	Key performance indicator
LoD	Level of Detail
RWS	Rural weather station
TMY	Typical meteorological year
UBEM	Urban building energy model/modeling
UBL	Urban boundary layer
UCL	Urban canopy layer
UHI	Urban heat island
UWG	Urban weather generator
UWS	Urban weather station
WMO	World Meteorological Organization

References

1. Department of Economic and Social Affairs, Population Division. *World Urbanization Prospects: The 2018 Revision*; United Nations: New York, NY, USA, 2019.
2. United Nations. *The Sustainable Development Goals Report 2022*; Lois Jensen: New York, NY, USA, 2019.
3. Salvati, A.; Kolokotroni, M. Urban Microclimate and Climate Change Impact on the Thermal Performance and Ventilation of Multi-Family Residential Buildings. *Energy Build.* **2023**, *294*, 113224. [[CrossRef](#)]
4. Ma, R.; Ren, B.; Zhao, D.; Chen, J.; Lu, Y. Modeling Urban Energy Dynamics under Clustered Urban Heat Island Effect with Local-Weather Extended Distributed Adjacency Blocks. *Sustain. Cities Soc.* **2020**, *56*, 102099. [[CrossRef](#)]
5. World Meteorological Organization. *Guidance on Measuring, Modelling and Monitoring the Canopy Layer Urban Heat Island (CL-UHI)*; World Meteorological Organization (WMO): Geneva, Switzerland, 2023; p. 101.
6. Oke, T.R. The Energetic Basis of the Urban Heat Island. *Q. J. R. Meteorol. Soc.* **1982**, *108*, 1–24. [[CrossRef](#)]
7. Battista, G.; Evangelisti, L.; Guattari, C.; Roncone, M.; Balaras, C.A. Space-Time Estimation of the Urban Heat Island in Rome (Italy): Overall Assessment and Effects on the Energy Performance of Buildings. *Build. Environ.* **2023**, *228*, 109878. [[CrossRef](#)]
8. De Cristo, E.; Evangelisti, L.; Battista, G.; Guattari, C.; De Lieto Vollaro, R.; Asdrubali, F. Annual Comparison of the Atmospheric Urban Heat Island in Rome (Italy): An Assessment in Space and Time. *Buildings* **2023**, *13*, 2792. [[CrossRef](#)]
9. Boccalatte, A.; Fossa, M.; Gaillard, L.; Menezo, C. Microclimate and Urban Morphology Effects on Building Energy Demand in Different European Cities. *Energy Build.* **2020**, *224*, 110129. [[CrossRef](#)]
10. Ni, X.; Chang, Y.; Bai, T.; Liu, P.; Song, H.; Wang, F.; Jin, M. Projections of Urban Heat Island Effects Under Future Climate Scenarios: A Case Study in Zhengzhou, China. *Remote Sens.* **2025**, *17*, 2660. [[CrossRef](#)]
11. Arnfield, A.J. Two Decades of Urban Climate Research: A Review of Turbulence, Exchanges of Energy and Water, and the Urban Heat Island. *Int. J. Climatol.* **2003**, *23*, 1–26. [[CrossRef](#)]

12. Mosteiro-Romero, M.; Schlueter, A. Effects of Occupants and Local Air Temperatures as Sources of Stochastic Uncertainty in District Energy System Modeling. *Energies* **2021**, *14*, 2295. [CrossRef]
13. Kamal, A.; Abidi, S.M.H.; Mahfouz, A.; Kadam, S.; Rahman, A.; Hassan, I.G.; Wang, L.L. Impact of Urban Morphology on Urban Microclimate and Building Energy Loads. *Energy Build.* **2021**, *253*, 111499. [CrossRef]
14. Reinhart, C.F.; Cerezo Davila, C. Urban Building Energy Modeling—A Review of a Nascent Field. *Build. Environ.* **2016**, *97*, 196–202. [CrossRef]
15. Borges, P.; Travasset-Baro, O.; Pages-Ramon, A. Hybrid Approach to Representative Building Archetypes Development for Urban Models—A Case Study in Andorra. *Build. Environ.* **2022**, *215*, 108958. [CrossRef]
16. Ferrando, M.; Causone, F.; Banfi, A.; Corrado, V.; Ballarini, I.; Piro, M.; Zarrella, A.; Carnieletto, L.; Borgato, N.; Evola, G.; et al. Developing an Italian Library of Reference Buildings for Urban Building Energy Modeling (UBEM): Lessons Learnt from the URBEM Project. *Energies* **2025**, *18*, 6026. [CrossRef]
17. Monteiro, C.S.; Pina, A.; Cerezo, C.; Reinhart, C.; Ferrão, P. The Use of Multi-Detail Building Archetypes in Urban Energy Modelling. *Energy Procedia* **2017**, *111*, 817–825. [CrossRef]
18. Johari, F.; Shadram, F.; Widén, J. Urban Building Energy Modeling from Geo-Referenced Energy Performance Certificate Data: Development, Calibration, and Validation. *Sustain. Cities Soc.* **2023**, *96*, 104664. [CrossRef]
19. Cerezo, C.; Sokol, J.; AlKhaled, S.; Reinhart, C.; Al-Mumin, A.; Hajiah, A. Comparison of Four Building Archetype Characterization Methods in Urban Building Energy Modeling (UBEM): A Residential Case Study in Kuwait City. *Energy Build.* **2017**, *154*, 321–334. [CrossRef]
20. Nakano, A.; Bueno, B.; Norford, L.; Reinhart, C. Urban Weather Generator—A Novel Workflow for Integrating Urban Heat Island Effect Within Urban Design Process. In *Proceedings of the Building Simulation 2015: 14th Conference of IBPSA*; IBPSA: Hyderabad, India, 2015; Volume 14, pp. 1901–1908.
21. Toparlar, Y.; Blocken, B.; Maiheu, B.; Van Heijst, G.J.F. A Review on the CFD Analysis of Urban Microclimate. *Renew. Sustain. Energy Rev.* **2017**, *80*, 1613–1640. [CrossRef]
22. Mochida, A.; Murakami, S.; Ojima, T.; Kim, S.; Ooka, R.; Sugiyama, H. CFD Analysis of Mesoscale Climate in the Greater Tokyo Area. *J. Wind Eng. Ind. Aerodyn.* **1997**, *67–68*, 459–477. [CrossRef]
23. Palme, M.; Inostroza, L.; Villacreses, G.; Lobato-Cordero, A.; Carrasco, C. From Urban Climate to Energy Consumption. Enhancing Building Performance Simulation by Including the Urban Heat Island Effect. *Energy Build.* **2017**, *145*, 107–120. [CrossRef]
24. Salvati, A.; Palme, M.; Chiesa, G.; Kolokotroni, M. Built Form, Urban Climate and Building Energy Modelling: Case-Studies in Rome and Antofagasta. *J. Build. Perform. Simul.* **2020**, *13*, 209–225. [CrossRef]
25. Li, X.; Zhou, Y.; Yu, S.; Jia, G.; Li, H.; Li, W. Urban Heat Island Impacts on Building Energy Consumption: A Review of Approaches and Findings. *Energy* **2019**, *174*, 407–419. [CrossRef]
26. Shen, P.; Wang, M.; Liu, J.; Ji, Y. Hourly Air Temperature Projection in Future Urban Area by Coupling Climate Change and Urban Heat Island Effect. *Energy Build.* **2023**, *279*, 112676. [CrossRef]
27. Shen, P.; Ji, Y.; Li, Y.; Wang, M.; Cui, X.; Tong, H. Combined Impact of Climate Change and Urban Heat Island on Building Energy Use in Three Megacities in China. *Energy Build.* **2025**, *331*, 115386. [CrossRef]
28. Hashemi, F.; Najafian, P.; Salahi, N.; Ghiasi, S.; Passe, U. The Impact of the Urban Heat Island and Future Climate on Urban Building Energy Use in a Midwestern U.S. Neighborhood. *Energies* **2025**, *18*, 1474. [CrossRef]
29. Jalali, Z.; Shamseldin, A.Y.; Ghaffarianhoseini, A. Urban Microclimate Impacts on Residential Building Energy Demand in Auckland, New Zealand: A Climate Change Perspective. *Urban Clim.* **2024**, *53*, 101808. [CrossRef]
30. Keppas, S.C.; Papadogiannaki, S.; Parliari, D.; Kontos, S.; Poupkou, A.; Tzoumaka, P.; Kelessis, A.; Zanis, P.; Casasanta, G.; de’Donato, F.; et al. Future Climate Change Impact on Urban Heat Island in Two Mediterranean Cities Based on High-Resolution Regional Climate Simulations. *Atmosphere* **2021**, *12*, 884. [CrossRef]
31. Lu, H.; Gaur, A.; Lacasse, M. Climate Data for Building Simulations with Urban Heat Island Effects and Nature-Based Solutions. *Sci. Data* **2024**, *11*, 731. [CrossRef]
32. Eyring, V.; Bony, S.; Meehl, G.A.; Senior, C.A.; Stevens, B.; Stouffer, R.J.; Taylor, K.E. Overview of the Coupled Model Intercomparison Project Phase 6 (CMIP6) Experimental Design and Organization. *Geosci. Model Dev.* **2016**, *9*, 1937–1958. [CrossRef]
33. CRiStAll. Homepage. Available online: <https://www.cristall.polito.it> (accessed on 16 December 2025).
34. Borelli, G.; Ballarini, I.; Corrado, V.; Gasparella, A.; Pernigotto, G. Assessment and Mapping of the Urban Heat Island Effect: A Preliminary Analysis on the Impact on Urban Morphology for the City of Turin, Italy. In *Proceedings of the Building Simulation Applications BSA 2024: 6th IBPSA-Italy Conference*; Bozen-Bolzano University Press: Bozen-Bolzano, Italy, 2024; pp. 525–531.
35. Joshi, M.Y.; Rodler, A.; Musy, M.; Guernouti, S.; Cools, M.; Teller, J. Identifying Urban Morphological Archetypes for Microclimate Studies Using a Clustering Approach. *Build. Environ.* **2022**, *224*, 109574. [CrossRef]
36. Javanroodi, K.; Perera, A.T.D.; Hong, T.; Nik, V.M. Designing Climate Resilient Energy Systems in Complex Urban Areas Considering Urban Morphology: A Technical Review. *Adv. Appl. Energy* **2023**, *12*, 100155. [CrossRef]
37. Bueno, B.; Norford, L.; Hidalgo, J.; Pigeon, G. The Urban Weather Generator. *J. Build. Perform. Simul.* **2013**, *6*, 269–281. [CrossRef]

38. Weng, Q.; Lu, D.; Schubring, J. Estimation of Land Surface Temperature–Vegetation Abundance Relationship for Urban Heat Island Studies. *Remote Sens. Environ.* **2004**, *89*, 467–483. [[CrossRef](#)]
39. Weng, Q. Thermal Infrared Remote Sensing for Urban Climate and Environmental Studies: Methods, Applications, and Trends. *ISPRS J. Photogramm. Remote Sens.* **2009**, *64*, 335–344. [[CrossRef](#)]
40. Zhou, D.; Xiao, J.; Bonafoni, S.; Berger, C.; Deilami, K.; Zhou, Y.; Frohling, S.; Yao, R.; Qiao, Z.; Sobrino, J.A. Satellite Remote Sensing of Surface Urban Heat Islands: Progress, Challenges, and Perspectives. *Remote Sens.* **2018**, *11*, 48. [[CrossRef](#)]
41. Deilami, K.; Kamruzzaman, M.; Liu, Y. Urban Heat Island Effect: A Systematic Review of Spatio-Temporal Factors, Data, Methods, and Mitigation Measures. *Int. J. Appl. Earth Obs. Geoinf.* **2018**, *67*, 30–42. [[CrossRef](#)]
42. Goldblatt, R.; Addas, A.; Crull, D.; Maghrabi, A.; Levin, G.G.; Rubinyi, S. Remotely Sensed Derived Land Surface Temperature (LST) as a Proxy for Air Temperature and Thermal Comfort at a Small Geographical Scale. *Land* **2021**, *10*, 410. [[CrossRef](#)]
43. Li, L.; Zha, Y.; Wang, R. Relationship of Surface Urban Heat Island with Air Temperature and Precipitation in Global Large Cities. *Ecol. Indic.* **2020**, *117*, 106683. [[CrossRef](#)]
44. ECOSTRESS. Homepage. Available online: <https://ecostress.jpl.nasa.gov/> (accessed on 10 October 2025).
45. Machard, A.; Salvati, A.; Tootkaboni, M.P.; Gaur, A.; Zou, J.; Wang, L.L.; Baba, F.; Ge, H.; Bre, F.; Bozonnet, E.; et al. Typical and Extreme Weather Datasets for Studying the Resilience of Buildings to Climate Change and Heatwaves. *Sci. Data* **2024**, *11*, 531. [[CrossRef](#)]
46. Reinhart, C.; Dogan, T.; Jakubiec, A.; Rakha, T.; Sang, A. Umi—An Urban Simulation Environment for Building Energy Use, Daylighting and Walkability. In *Proceedings of the Building Simulation 2013: 13th Conference of IBPSA, Chambéry, France, 25–28 August 2013; Volume 13*, pp. 476–483.
47. Dogan, T.; Reinhart, C. Shoeboxer: An Algorithm for Abstracted Rapid Multi-Zone Urban Building Energy Model Generation and Simulation. *Energy Build.* **2017**, *140*, 140–153. [[CrossRef](#)]
48. *EN ISO 7730*; Ergonomics of the Thermal Environment. Analytical Determination and Interpretation of Thermal Comfort Using Calculation of the PMV and PPD Indices and Local Thermal Comfort Criteria. European Committee for Standardization (CEN): Brussels, Belgium, 2006.
49. *EN 16798-1*; Energy Performance of Buildings. Ventilation for Buildings Indoor Environmental Input Parameters for Design and Assessment of Energy Performance of Buildings Addressing Indoor Air Quality, Thermal Environment, Lighting and Acoustics. Module M1-6. European Committee for Standardization (CEN): Brussels, Belgium, 2019.
50. Hamdy, M.; Carlucci, S.; Hoes, P.-J.; Hensen, J.L.M. The Impact of Climate Change on the Overheating Risk in Dwellings—A Dutch Case Study. *Build. Environ.* **2017**, *122*, 307–323. [[CrossRef](#)]
51. *EN ISO 52000-1*; Energy Performance of Buildings. Overarching EPB Assessment. Part 1: General Framework and Procedures. European Committee for Standardization (CEN): Brussels, Belgium, 2017.
52. *EN ISO 52016-1*; Energy Performance of Buildings. Energy Needs for Heating and Cooling, Internal Temperatures and Sensible and Latent Heat Loads Calculation Procedures. European Committee for Standardization (CEN): Brussels, Belgium, 2017.
53. *CEN/TR 16798-2*; Energy Performance of Buildings. Ventilation for Buildings Interpretation of the Requirements in EN 16798-1. Indoor Environmental Input Parameters for Design and Assessment of Energy Performance of Buildings Addressing Indoor Air Quality, Thermal Environment, Lighting and Acoustics (Module M1-6). European Committee for Standardization (CEN): Brussels, Belgium, 2019.
54. *EN ISO 15927-6*; Hygrothermal Performance of Buildings. Calculation and Presentation of Climatic Data Accumulated Temperature Differences (Degree Days). European Committee for Standardization (CEN): Brussels, Belgium, 2008.
55. Oke, T.R. City Size and the Urban Heat Island. *Atmos. Environ.* **1973**, *7*, 769–779. [[CrossRef](#)]
56. Ballarini, I.; Piro, M.; Corrado, V.; Pernigotto, G.; Borelli, G.; Gasparella, A. A Methodology for the Assessment of the Urban Heat Island Effect by Exploiting the Urban Archetype Approach. In *Proceedings of the 15th REHVA HVAC World Congress—CLIMA 2025; Lecture Notes in Civil Engineering*; Zilio, C., Busato, F., Mazzarella, L., Noro, M., Eds.; Springer Nature Switzerland: Cham, Switzerland, 2026; Volume 763, pp. 1179–1191.
57. OpenStreetMap. Homepage. Available online: <https://www.openstreetmap.org> (accessed on 18 December 2025).
58. Geoportal of the Metropolitan City of Turin. Homepage. Available online: <http://geoportale.comune.torino.it/web/> (accessed on 10 October 2025).
59. Robinson, D.; Haldi, F.; Kämpf, J.; Leroux, P.; Perez, D.; Rasheed, A.; Wilke, U. CitySim: Comprehensive Micro-Simulation of Resource Flows for Sustainable Urban Planning. In *Proceedings of the International Building Performance Simulation Association Conference (IBPSA 2009)*; IBPSA: Glasgow, Scotland, 2009; Volume 11, pp. 1083–1090.
60. Ballarini, I.; Piro, M.; Tootkaboni, P.M. Procedures and Services to Undertake Large-Scale Statistical Analysis of EPCs Databases. Transversal Deployment Scenario 5. TIMEPAC Deliverable 2.5. Available online: <https://timepac.eu/reports/procedures-and-services-to-undertake-large-scale-statistical-analysis-of-epcs-databases/> (accessed on 10 October 2025).
61. *UNI EN 16798-1:2019/NA:2025*; Italian National Annex of the EN 16798-1. Italian Organisation for Standardisation (UNI): Milan, Italy, 2025.

62. ARPA Piemonte. Homepage. Available online: <https://www.arpa.piemonte.it/> (accessed on 10 October 2025).
63. UNI 10349-3; Riscaldamento e Raffrescamento degli Edifici. Dati Climatici. Differenze di Temperatura Cumulate (Gradi Giorno) ed altri Indici Sintetici. Italian Organisation for Standardisation (UNI): Milan, Italy, 2016. (In Italian)

Disclaimer/Publisher's Note: The statements, opinions and data contained in all publications are solely those of the individual author(s) and contributor(s) and not of MDPI and/or the editor(s). MDPI and/or the editor(s) disclaim responsibility for any injury to people or property resulting from any ideas, methods, instructions or products referred to in the content.